



Modification, Characterization and Evaluation of a Quantum / Interband Cascade Laser Spectrometer for simultaneous airborne in situ observation of CH₄, C₂H₆, CO₂, CO and N₂O

Julian Kostinek¹, Anke Roiger¹, Kenneth J. Davis³, Colm Sweeney⁶, Joshua P. DiGangi⁵, Yonghoon Choi^{5,7}, Bianca Baier^{6,8}, Frank Hase⁴, Jochen Groß⁴, Maximilian Eckl¹, Theresa Klausner¹, and André Butz²

¹Deutsches Zentrum für Luft- und Raumfahrt, Institut für Physik der Atmosphäre, Oberpfaffenhofen, Germany

²Institute of Environmental Physics, University of Heidelberg, Heidelberg, Germany

³Department of Meteorology and Atmospheric Science, The Pennsylvania State University, University Park, PA 16802, USA

⁴Institute of Meteorology and Climate Research, Karlsruhe Institute of Technology, Karlsruhe, Germany

⁵NASA Langley Research Center, Hampton, VA 23681-2199, USA

⁶NOAA ESRL Global Monitoring Division, Boulder, CO 80305-3328, USA

⁷Science Systems and Applications, Inc., Hampton, VA 23681, USA

⁸Cooperative Institute for Research in Environmental Sciences, University of Colorado Boulder, Boulder, CO 80305, USA

Correspondence: Julian Kostinek (julian.kostinek@dlr.de)

Abstract. Achieving an improved understanding of the anthropogenic influence on climate due to man made greenhouse gas emissions is of major interest for the global civilization. Sources, sinks and transport of climatologically-relevant gases in the Earth's atmosphere are still insufficiently understood, implying a fundamental need for accurate, spatially and temporally dense observations. Tunable diode laser absorption spectroscopy is a widely used technique for in situ sensing of atmospheric composition. Mid-infrared spectrometers have become commercially available, since continuous wave quantum cascade (QCL) and interband cascade lasers (ICL) today achieve excellent performance, stability and high output power at typical ambient conditions. Aircraft deployment poses a challenging environment for these newly-developed instruments. Here, we demonstrate the successful adaption of a commercially available QCL/ICL based spectrometer for airborne in-situ trace gas measurements. The instrument measures methane, ethane, carbon dioxide, carbon monoxide, nitrous oxide and water vapor simultaneously, with high 1σ -precision (740 ppt, 205 ppt, 460 ppb, 2.2 ppb, 137 ppt, 16 ppm, respectively) and high frequency (2 Hz). We estimate a total measurement uncertainty of 2.3 ppb, 1.6 ppb, 1.0 ppm, 7.4 ppb and 0.8 ppb in CH₄, C₂H₆, CO₂, CO and N₂O, respectively. The instrument enables truly simultaneous and continuous (zero dead-time) observations for all targeted species. Frequent calibration allows for a measurement duty cycle $\geq 90\%$ while retaining high accuracy. A custom retrieval software has been implemented and instrument performance is reported for a first field deployment during NASA's Atmospheric Carbon and Transport America (ACT-America) campaign in fall 2017 over the eastern and central U.S.. This includes an inter-instrumental comparison with a calibrated cavity ring-down greenhouse gas analyzer (operated by NASA Langley Research Center, Hampton, USA) and periodic flask samples analyzed at the National Oceanic and Atmospheric Administration (NOAA). We demonstrate excellent agreement of the QCL/ICL based instrument to these concurrent observations within the combined measurement uncertainty.



1 Introduction

With steadily increasing greenhouse gas concentrations in the Earth's atmosphere an improved understanding of the anthropogenic influence on climate is of major interest for the global civilization. Globally averaged carbon dioxide (CO_2) mixing ratios have increased by 40% since 1750. Methane (CH_4) mixing ratios have more than doubled since the pre-industrial era, where over 60% of this increase is estimated to be of anthropogenic nature (IPCC, 2014). Nitrous oxide (N_2O) is a strong greenhouse gas and is expected to remain the most important ozone-depleting anthropogenic impact throughout the 21st century (Ravishankara et al., 2009). Ethane (C_2H_6) is a powerful tracer commonly used to discriminate between different types of methane sources (Smith et al. (2015); Barkley et al. (2017); Peischl et al. (2015)) and carbon monoxide (CO) is a marker for incomplete combustion processes and relates to the formation of tropospheric ozone (Klemm et al., 1996).

Aircraft provide a flexible basis for satisfying the fundamental need for accurate, temporally and spatially dense observations of these climatologically-relevant gases from local to regional scales. On-board meteorological data acquisition systems allow for concurrent observations of important atmospheric state variables like the local wind field, which is particularly useful to estimate emission fluxes. Spectroscopic instruments making use of molecular ro-vibrational absorption allow for high temporal coverage through fast instrument response times (Chen et al., 2010). Some have already been used for airborne research, e.g. well-established cavity ring-down instruments (O'Shea et al. (2013); Santoni et al. (2014); Cambaliza MOL (2015); Filges et al. (2015)). With the commercial availability of continuous-wave lasers emitting in the mid infrared (IR) region near ambient temperature (Capasso (2010); Vurgaftman et al. (2015); Kim et al. (2015), Beck et al. (2002)) several new instrument designs have emerged (McManus et al. (2015); Zellweger et al. (2016)). QCL/ICL based systems exploit several orders of magnitude stronger molecular absorption features in the mid infrared compared to near infrared based cavity ring-down instruments. Richter et al. (2015) reported on a custom-built QCL spectrometer for simultaneous in-situ detection of formaldehyde (CH_2O) and C_2H_6 providing best-in-class detection sensitivities of 40 ppt and 15 ppt, respectively. The custom-built airborne QCL spectrometer described by Catoire et al. (2017) allows for simultaneous observation of CO , CH_4 and nitrogen dioxide (NO_2) with in-flight precisions of 0.3 ppb, 5 ppb and 0.3 ppb for a sampling time of 1.6 s. McManus et al. (2011) reported on the development of a high-sensitivity trace gas instrument based on quantum cascade lasers and astigmatic Herriott cells with up to 240 m path length. This design is commercially available from AERODYNE RESEARCH INC., Billerica, USA, and allows for simultaneous observation of a multitude of gases, depending on the wavelength of the installed lasers. Unlike many established cavity ring-down instruments measuring different species sequentially, the described spectrometer allows for truly concurrent sensing of the selected observables and faster response times. These instruments have already been operated on different research aircraft. Santoni et al. (2014) reported on overall instrument performance for over 500 flight hours. Pitt et al. (2016) found a strong cabin pressure dependence on retrieved methane mixing ratios. Recently, Gvakharia et al. (2018) described a fast calibration strategy to overcome this cabin pressure dependence.

Here, we describe the setup and performance of our flight-proven (over 100 flight hours) airborne QCL/ICL system developed for simultaneous airborne measurements of CH_4 , C_2H_6 , CO_2 , CO , N_2O and H_2O . Section 2 summarizes the refinements over the commercial system for use on aircraft. We show that frequent two-point calibration can mitigate cabin pressure de-



pendencies. Section 3 describes our custom-built retrieval software developed for tuning the retrieval process to yield optimum output. Sections 4 and 5 report on instrument performance in the laboratory and in the field during NASA's ACT-America fall 2017 campaign, respectively, including an inter-instrumental comparison with a calibrated cavity ring-down instrument and periodically taken flask samples. Section 6 summarizes our findings and concludes the study.

5 2 The airborne DLR QCL/ICL spectrometer

The spectrometer system used here builds upon the *Dual Laser Trace Gas Monitor*, a commercial tunable IR laser diode absorption spectrometer (TILDAS) available from *AERODYNE RESEARCH INC., Billerica, USA*. The basic instrument has already been extensively described in McManus et al. (2011). We will therefore only briefly introduce the basic instrument setup followed by a description of the refinements required to operate the instrument on research aircraft.

10 2.1 Basic instrument setup

The spectrometer is split into an electronics compartment and an optics compartment. The electronics compartment includes an embedded computing system, thermoelectric cooling (TEC) controllers, power supplies, etc.. The optics compartment includes the lasers, the sample cell, the pressure controller and all optical elements.

Fig. 1 shows a top-view photograph of the optics compartment. A combination of a continuous wave (CW) QCL and ICL
15 measures mixing ratios of CH_4 , C_2H_6 , CO_2 , CO , N_2O and H_2O simultaneously by direct absorption spectroscopy. The sample cell is an astigmatic Herriott cell with approximate physical dimensions of 15cm x 15cm x 50cm (WxHxL) made from

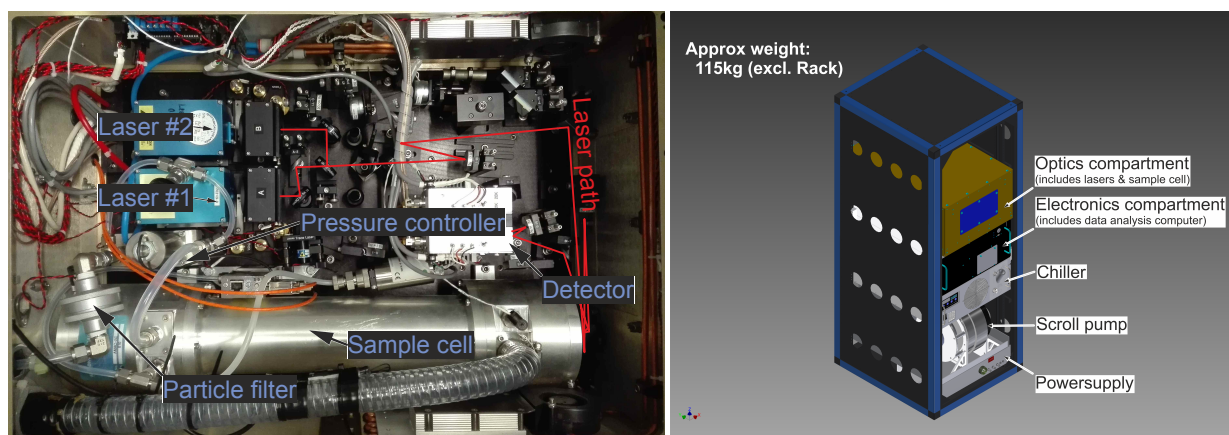


Figure 1. Top-down photograph on the optics compartment (left panel). The sample cell made from aluminum along with the pressure controller and pressure transducers can be identified in the lower half. The QCL/ICL lasers are mounted inside the blue housings to the left of the collimating Schwarzschild telescopes in the two black housings. The two detectors are mounted below the silver aluminum cases, housing the pre-amplifiers, on the right. The first detector is used for detecting both lasers after passing through the sample cell. The second detector is used for spectral referencing through an auxiliary optical path. The right panel illustrates the rack mounted instrument.



aluminum. It provides an effective absorption path length of 204m with a net volume of 2.1 L. Two laser light sources emit in the mid-IR region, specifically around 3.3 μm for Laser #1 and 4.5 μm for Laser #2. Both lasers are tuned to a specific center wavelength by adjusting the temperature using Peltier elements directly attached to the laser diodes. Excess heat is removed through a liquid cooling/heating circuit (*SOLID STATE COOLING SYSTEMS, New York, USA*). Operating temperatures are

5 4.7°C for Laser #1 and 1.5°C for Laser #2, respectively. A linear current ramp drives sequential spectral modulation at a fixed frequency of 1.5 kHz. Laser #1 is tuned between 2988.520 cm^{-1} and 2990.625 cm^{-1} . The second laser is tuned between 2227.550 cm^{-1} and 2228.000 cm^{-1} . Laser #1 scans over absorption lines of CH_4 , C_2H_6 and H_2O , the second laser sweeps over N_2O , CO_2 and CO lines. Each laser is sampled at 450 spectral points. Acquired spectra are co-added to yield a single output spectrum every half of a second. Before reaching the sample cell, the laser beam travels approximately 1.6m inside the

10 instrument under ambient conditions. This will be referred to as the open-path of the instrument, which is heavily influenced by variations in cabin pressure, temperature and humidity during airborne operation. After passing through the sample cell, the combined output from both lasers hits a single TEC-cooled detector. A second, identical detector collects radiation from two auxiliary paths. The first auxiliary path contains a small, sealed reference cell filled with CH_4 and N_2O . This allows for spectral referencing during system startup. The second path introduces an etalon into the beam, allowing for experimental

15 determination of the laser tuning rate, which relates laser supply current and emitted wavelength.

2.2 Refinements for airborne operation

The key challenges for a successful deployment on research aircraft are limited space and power, the occurrence of linear and angular accelerations and large pressure, temperature and humidity fluctuations in both cabin and sampled air. Airborne instrumentation further requires a fast system response time, owing to the rapid movement of aircraft in the atmosphere. The

20 response time is controlled by the time it takes to completely exchange the air in the sample cell which is driven by the highest achievable volumetric flow rate given a specific pump and sample cell volume.

Here, a scroll pump has been chosen to enable a constant sample flow through the sample cell. The lubricant-free scroll pump runs very smoothly, avoiding injecting large vibrations into the measurement system, yet providing good pumping performance with a nominal value of 500 liters per minute at standard conditions. This translates to a net flow rate of 25 SLPM when

25 operating with a cell pressure of 50 hPa. Earlier experience showed that large electrical inrush currents have jeopardized nominal system startup (priv. comm. Stefan Müller, MPI Mainz). The original motor has therefore been exchanged with a synchronous three-phase motor (*BAUMUELLER NUERNBERG GMBH, Velbert, Germany*). This DC motor provides a rated power of 627 W at 28 VDC. By using a digital motor controller the maximum startup current can be limited amongst various other tuning options. From previous studies the motor is known to emit a considerable amount of heat; a forced airflow provided

30 by a standard axial fan ensures motor temperatures stay in the rated range.

Aircraft deployment requires the entire system to operate with a maximum of 50 A at 28 VDC. Power consumption of the instrument is mainly dominated by the pump and the thermoelectric cooling making up more than 3/4 of the total power requirement. Both components have been electrically converted without the need for power inverters from 230 V AC to 28 V DC to increase overall efficiency. The spectrometer and its internal computer are driven by a power inverter.



Large parts of the wiring harness have been exchanged from standard PVC cables to aviation-grade fire-resistant wiring. Mandatory electromagnetic compatibility/interference (EMC/EMI) tests have been carried out to comply with Federal Aviation Administration (FAA) regulations. The rack-mounted instrument sums up to a total mass of approx. 115 kg and has been tested to withstand linear accelerations of up to 9g on the aircraft forward axis, 8g on the downward axis, 6g on the upward and 2.25g
5 sideways. Due to aircraft certification issues, pure water is used as process fluid for the liquid cooling/heating circuit instead of the intended propylene glycol / water mixture.

A 3/8" inner diameter hose made out of Polytetrafluoroethylene (PTFE) has been chosen for the sample air intake as a compromise between pressure drop across the inlet and to minimize lag time between the inlet and the sample cell. Inside the instrument and upstream of the sample cell, an aerosol filter holds back particles bigger than 2 μm. The inlet is rear facing,
10 preventing large particle entrainment and protecting the instrument from liquid water and ice. Owing to the small diameter, the intake flow is inside the turbulent regime at all times ($Re \sim 4000$).

Finally, the sample cell pressure is regulated by means of a fully-configurable pressure controller (*BRONKHORST High-Tech B.V., Ruurlo, Netherlands*). A chip-scale temperature-compensated pressure transducer (*Measurement Specialties (Europe), Ltd.*) and a humidity sensor (*Sensirion AG, Staefa ZH, Switzerland*) have been built into the optics compartment, to allow for
15 monitoring the open path state variables (see section 2.1).

2.3 In-flight calibration strategy

A custom-built calibration system has been implemented as illustrated in Fig. 2. Using mass flow controllers (MFCs, *BRONKHORST High-Tech B.V., Ruurlo, Netherlands*), two gases can be mixed at arbitrary ratios. The calibration gas mixture has been chosen to resemble "target" gas mixing ratios close to atmospheric ambient conditions. The cylinders have been cross-calibrated
20 against NOAA standards and are thus traceable to World Meteorological Organization (WMO) standards for the species CH_4 and CO_2 . C_2H_6 , CO and N_2O are compared to NOAA flask samples taken during the ACT-America field campaigns, which are also traceable to WMO standards. We use ultra-pure synthetic air as "zero" gas instead of pure nitrogen (N_2) to be in accordance with aircraft safety regulations and because the mixing ratio of synthetic air (79.5% N_2 and 20.5% O_2) is chemically closer to sampled atmospheric air. Our calibration setup allows the net flow rate from the calibration cylinders to be
25 slightly higher than the sample flow rate, minimizing pressure variations in the sample cell during switchover from normal to calibration sampling. To avoid contamination with cabin air, leak tests have been carried out on a regular basis during the ACT-America field campaign.

Owing to the high sensitivity of the retrieved mixing ratios to changes in ambient conditions during flights (Gvakharia et al., 2018), calibration cycles are carried out automatically every 5 to 10 minutes. Each cycle consists of a pre-programmed sequence of flushing the sample cell with zero gas for 10 seconds followed by another 10 seconds of calibration gas. These time
30 intervals have been found to be a good compromise between calibration gas cylinder endurance and measurement duty cycle. Furthermore, only a single MFC is active at the time for in-flight calibration, reducing the uncertainty on the calibration gas mixing ratios to the uncertainties on the gas cylinders themselves. Online mixing (only relevant for linearity checks, not for in-flight calibration) adds the uncertainty of the controlled mass flow on top. Measured mixing ratios of all detected species

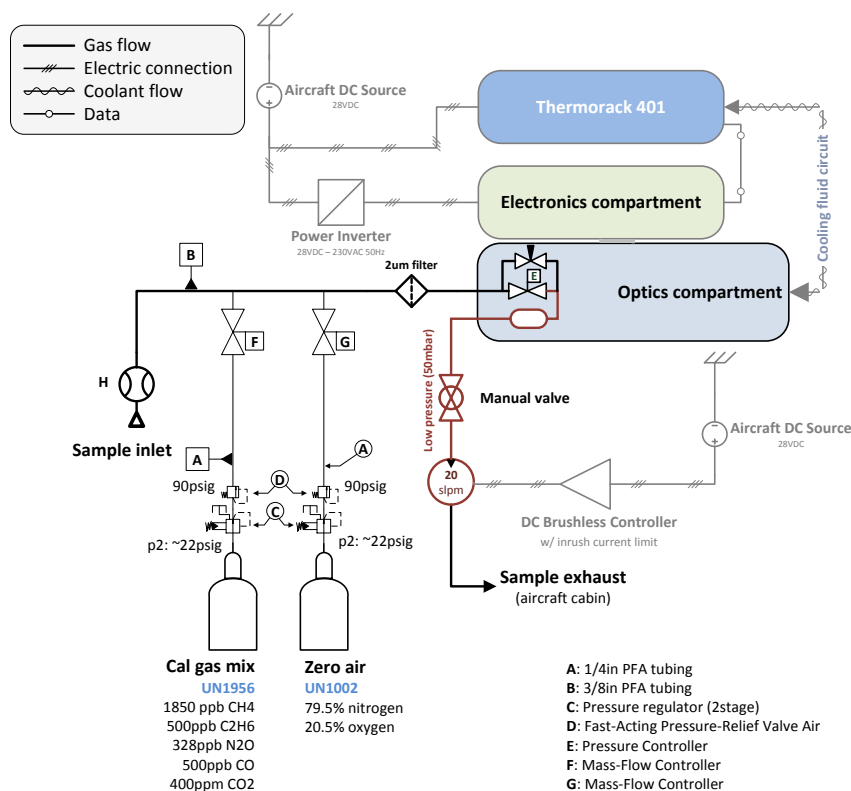


Figure 2. Schematic showing the main components with emphasis on the calibration system. A mass flow meter allows for measuring the sample flow rate. Two reference gases can be mixed at any arbitrary ratio by means of two calibrated mass flow controllers. A $2\mu\text{m}$ particle filter upstream of the sample cell avoids cell contamination.

settle to an approximately constant value within the first two seconds after switchover from calibration gas to sample air and vice versa. The only exception is water vapor, which is observed to settle after approx. 30 seconds because of its stickiness and because the inlet tubing is made out of PTFE. The observed decay in H_2O is different from the decay in other species in that a slow, almost linear decay follows the initial exponential decay, due to remaining water vapor in the inlet tubing and the sample cell.

3 Data Retrieval & Post-processing

The standard approach to retrieve dry-air mixing ratios from the Aerodyne QCLS instruments is by making use of the software supplied by the manufacturer (TDLWintel). Here we utilize a custom retrieval software (JFIT) developed to double check the output of the TDLWintel software and to enhance the ability of tweaking the retrieval process to yield optimum output.



- The code is written in plain C++. It digests the sample cell pressure and temperature measurements to generate a synthetic spectrum based on line-by-line parameters from the HITRAN2012/HITRAN2016 (Rothman et al. (2013); Gordon et al. (2017)) database using a conventional Voigt profile approach. Ethane line-by-line data have been taken from high-resolution FTIR spectra due to deficiencies in the HITRAN data for this particular species/wavenumber combination (Harrison et al., 2010).
- 5 The computation of the Voigt profile has been adopted from Abrarov and Quine (2015) for improved efficiency. Our retrieval code differs from the TDLWintel approach in the determination of the spectral baseline, the handling of shift parameters and open path water absorption. TDLWintel's spectral baseline is defined by manually positioned markers and shift parameters are specific for each species and coupled to a fingerprint absorption line (see Fig. 4). Determination of open path water absorption is only possible at one fixed pressure value.
- 10 A typical raw spectral output, as saved by the instrument in binary format is illustrated in Fig. 3. The two consecutive laser scans are clearly visible. On the left side, Laser #1 sweeps between 2988.520 cm^{-1} and 2990.625 cm^{-1} and hence, over absorption features of CH_4 , C_2H_6 and H_2O . The right side corresponds to the wavelength range of Laser #2 (2227.550 cm^{-1} to 2228.000 cm^{-1}) and includes absorption features of N_2O , CO and CO_2 . After the lasers have scanned their full range, both lasers are completely turned off to allow for the determination of the detector zero-intensity offset. The abscissa corresponds
- 15 to the individual sampling points, which can be converted to spectral units using the known laser tuning rate. The flat sections

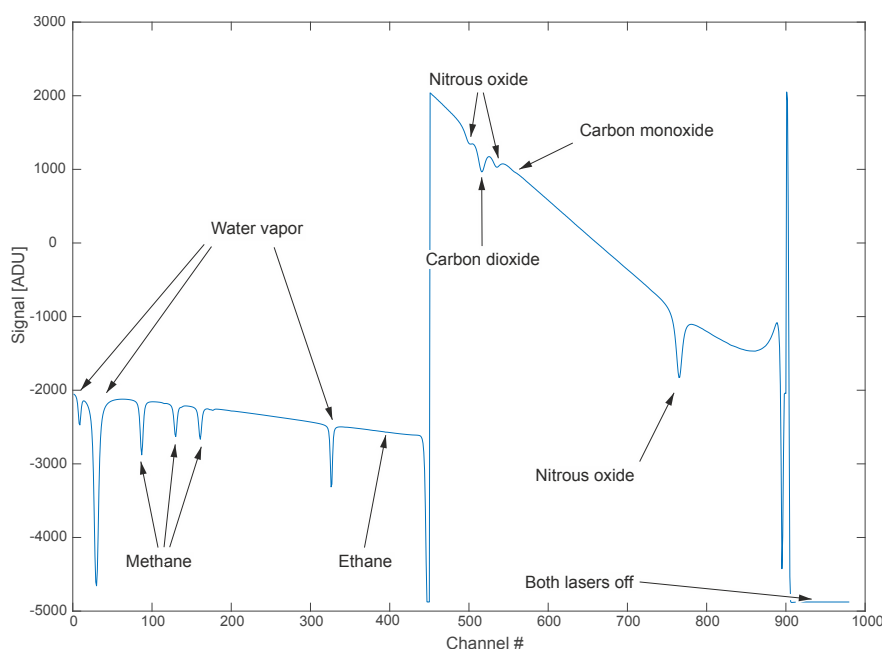


Figure 3. A typical raw spectrum as recorded in binary format by the instrument. Arrows have been added to ease identification of the observed chemical species. Channel numbers on the abscissa can be converted to spectral units using the laser tuning rate. The intensity offset can be corrected by shifting the entire spectrum to yield zero intensity when lasers are turned off.

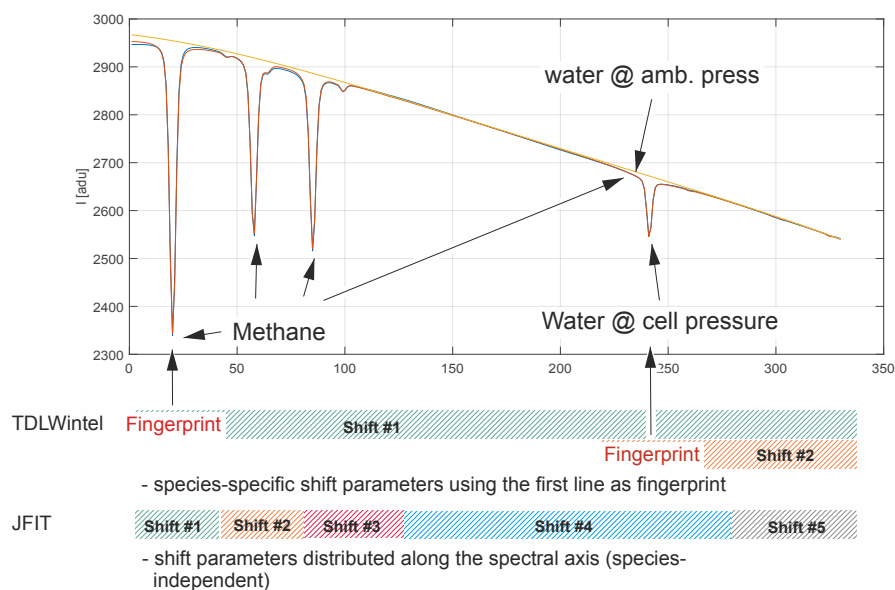


Figure 4. Schematic depicting the handling of spectral shift parameters and baseline modeling. The spectral baseline is fitted as a polynomial together with absorption features over the entire micro window. Shift parameters have been implemented in a species-independent way. Open-path water is also included in the model.

of the spectrum with no molecular absorption, are considered to represent the spectral baseline. The shape of this baseline is mainly controlled by laser characteristics, the detector response function and optical properties of the installed mirrors and windows inside the instrument.

The spectrum is broken down into 3 micro windows for the retrieval process (see Fig. 5). These were chosen based on best overall performance found in retrieval tests and named after the chemical species included. A synthetic spectrum, including a polynomial representing the spectral baseline, is generated and fitted using an unbounded Levenberg-Marquardt least-squares algorithm (Marquardt, 1963). The degree of the background-fitting polynomial has been adjusted empirically for each micro window. Species independent shift parameters have been included allowing individual absorption features to freely move on the spectral axis. Special care has been taken to group weak and strong absorption features together in a single shift parameter, to provide sufficient certainty on their spectral positions. In other words, not every absorption line has its own shift parameter, but they are grouped as schematically shown in Fig. 4. As a result, only 5 shift parameters are included although the synthetic spectrum in Fig. 4 is composed of more than 20 individual lines. When the absorptivity does not yield enough certainty to ensure proper determination of the shift parameters for a single spectrum, the shift variables are held constant at the mean over its last 10 values. If another species in the relevant micro window allows for a proper determination of the spectral position, remaining shift parameters are coupled to those with enough certainty. This strategy allows to properly model frequency changes between consecutive measurements. Typical shift parameters for ground-based operation are given in Fig. 8 for the CH_4 - H_2O and



CO_2 - CO - N_2O micro windows. Pressure, humidity and temperature data obtained from within the optics compartment are used to model H_2O absorption at cabin pressure in the open-path region.

The CH_4 - H_2O micro window covers almost the entire set of spectral features covered with Laser #1 except for the C_2H_6 absorption features. The spectral baseline is modeled as a third-order polynomial over the full range of the micro window. A typical spectrum including fit is depicted in Fig. 5 along with typical spectra for the other two micro windows.

The C_2H_6 micro window includes absorption features of CH_4 and C_2H_6 . The main challenge of retrieving precise C_2H_6 mixing ratios arises from its very low background concentration in the atmosphere (approx. 1.05 ppb in the northern hemisphere

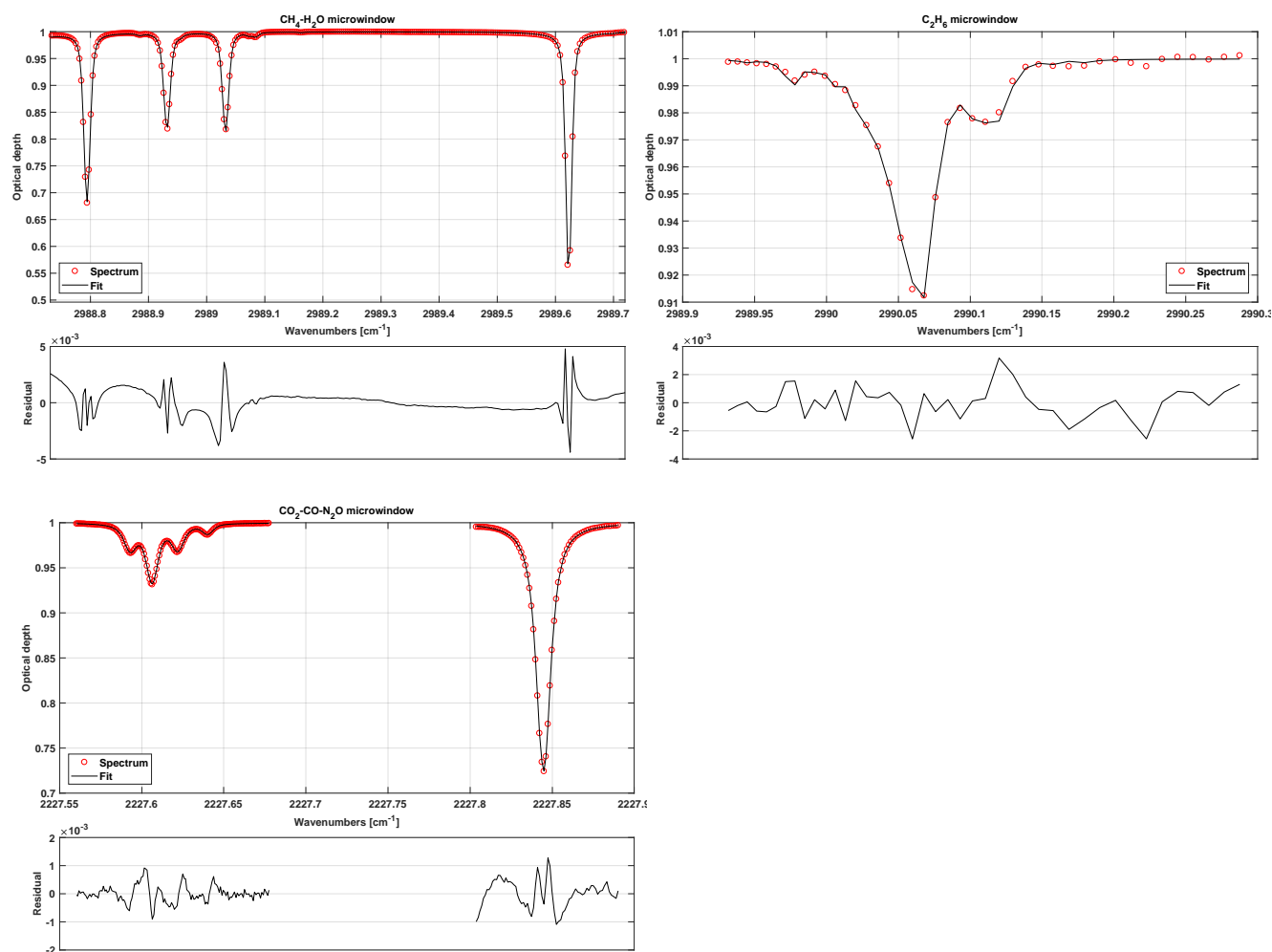


Figure 5. Typical, normalized spectra for each micro window including fits and associated residuals. The first micro window (top left) includes CH_4 and H_2O absorption features. The top right micro window depicts C_2H_6 absorption. The lower left spectrum shows CO , CO_2 and N_2O absorption.



(Simpson et al., 2012)). A single adjacent CH_4 line has been included in order to obtain good C_2H_6 data even under these challenging conditions. In this case, the weak CH_4 absorption is not modeled as a free parameter and is hence not used for retrieving the CH_4 mixing ratio, but for localizing the spectral position / shift parameter of the C_2H_6 absorption feature in the absence of a clear C_2H_6 signal. The CH_4 mixing ratios are fixed to the values determined from the previous micro window.

5 Using this approach, we found a clear improvement in the C_2H_6 data quality including a higher precision and the absence of discontinuities. The associated spectral baseline is modeled as a second-order polynomial.

The CO_2 - CO - N_2O micro window covers the entire second laser and is the most complex spectral scene. It includes several overlapping absorption features making the retrieval of mixing ratios of the targeted species challenging. As illustrated in Fig. 5, a single CO_2 absorption line is surrounded by two N_2O lines. The CO line is directly adjacent to one of the N_2O lines. This

10 results in comparatively large signal noise and deteriorated accuracy on the retrieved mixing ratios due to crosstalk between the N_2O , CO and CO_2 absorption lines. However, the spectral range includes another N_2O line at 2227.843 cm^{-1} , which is slightly stronger than the other two (see Fig. 5). Our approach is to fix the mixing ratios of the first two N_2O lines to the stronger third one, in order to reduce the uncertainty on retrieved N_2O and hence the noise on the CO_2 and CO retrieval. The

15 CO_2 absorption line originates from a molecular transition of the $^{13}C^{16}O_2$ carbon dioxide isotopologue, resulting in reduced accuracy if the isotopic composition of the sample is not accurately constrained. The spectral baseline has been split into two parts, the first covering the first two N_2O , CO_2 and CO lines, and the second covering the individual N_2O line only. Both are modeled as second-order polynomials.

3.1 Water vapor correction

In the current instrument setup, water vapor is not removed from sampled air before entering the sample cell. Therefore, the

20 influence of water vapor on the retrieved mixing ratios has to be corrected in order to report dry-air mixing ratios. Here, we correct for both, dilution and water broadening effects. The first describes the fact that concentrations appear smaller when analyzing moist air, although the dry air mole fraction might be constant. This effect can be remedied for if the absolute water concentration is known for each individual sample using Eq. 1

$$c_d = \frac{c_x}{(1 - c_{H_2O})} \quad (1)$$

25 where c_d is the dry-air mole fraction, c_x is the raw concentration of a particular species of interest diluted in moist air and c_{H_2O} is the water vapor concentration (Harazono et al., 2015). Spectroscopic water broadening effects are approximately an order of magnitude smaller than dilution effects, yet they do have to be corrected for to obtain precise measurements. HITRAN's air broadening parameters are listed for a particular chemical composition of air excluding water vapor. H_2O , however, can be a more potent broadening agent than nitrogen or oxygen (Kooijmans et al., 2016). These coefficients have been determined using

30 the setup depicted in Fig. 6 and are summarized in Tab. 1. Therefore, the pressure broadening has to be modified to include this effect. Under dry air conditions it is common to split the pressure broadening into two parts: self-broadening and air-broadening. The self-broadening coefficient allows computation of the broadening induced by mutual collisions of a particular species of interest. The air-broadening coefficient can be used to approximate the broadening induced through collisions of a



Table 1. Empirically determined water vapor foreign broadening coefficients

Chemical species	CH_4	C_2H_6	CO_2	CO	N_2O
Broadening coefficient $\times \gamma_{air}$	1.05	1.18	2.2	2.1	2.2

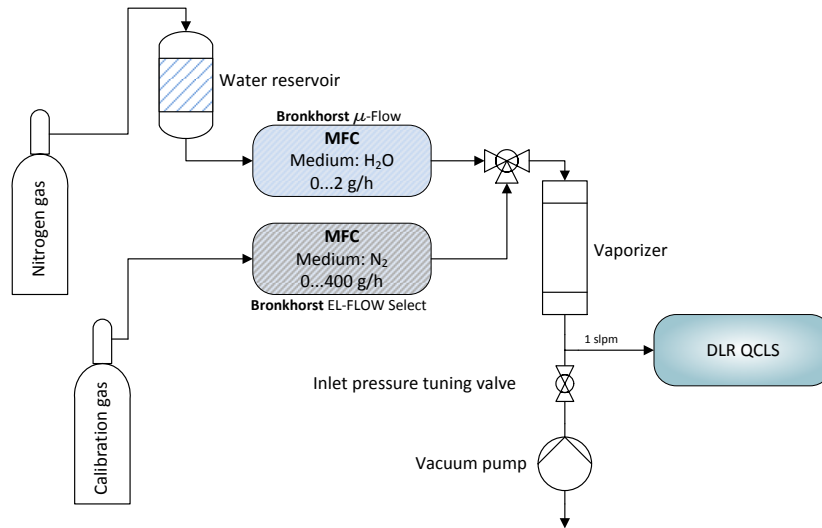


Figure 6. Schematic depicting the water correction lab setup. A reference gas can be humidified to typical atmospheric values between 0% and 2% absolute water using mass flow controllers and an electronically controlled vaporizer. A downstream pump allows for simulation of different flight levels.

particular species with all the other species in a given air standard excluding the species itself. From the HITRAN definitions, the pressure-broadened half width at half maximum for a gas at pressure p and temperature T is given by

$$\gamma(p, T) = \left(\frac{T_{ref}}{T} \right)^{n_{air}} (\gamma_{air}(p - p_{self}) + \gamma_{self}p_{self}) \quad (2)$$

where T_{ref} is a fixed reference temperature ($T_{ref} = 296 K$), p_{self} is the partial pressure of a particular species of interest and n_{air} is the coefficient of the temperature dependence of the air-broadened half width. This model has been extended to include collisions with H_2O molecules yielding

$$\gamma(p, T) = \left(\frac{T_{ref}}{T} \right)^{n_{air}} (\gamma_{air}(p - p_{self} - p_{H_2O}) + \gamma_{self}p_{self} + \gamma_{H_2O}p_{H_2O}) \quad (3)$$

with the partial pressure of water vapor p_{H_2O} and the water broadening coefficient γ_{H_2O} . The former can be computed from the measured water vapor concentration. The latter can be empirically determined. Two MFCs are used to precisely modify mixing ratios of water vapor in a clean and dry calibration gas. Theoretical computation of the water vapor mole fraction follows under the assumption that there is no water deposition on the enclosing flow channel surfaces and therefore the existence of a steady



state flow condition. The amount of each constituent n in mols can be computed using the mass flow rate \dot{m} (integrated over a suitable interval of time) and the corresponding molar mass M . An additional downstream pump allows, in combination with a manually-controlled needle-valve, tuning the absolute pressure at the instrument inlet to simulate altitude changes. For these tests, the QCLS instrument has been operated at low flow rates of approx. 1 *SLPM* due to limitations on the two mass flow controllers. The water broadening coefficient γ_{H_2O} has been adjusted iteratively until reported dry-air mixing-ratios of the species of interest remained constant for the set of water vapor mixing ratios.

4 Ground-based performance

Extensive ground-based instrument checks have been conducted, including tests in a pressure chamber at the Karlsruhe Institute of Technology (KIT) and laboratory tests at DLR Oberpfaffenhofen, Germany. These tests confirmed the presence of an ambient pressure dependence found in earlier studies (i.e. Pitt et al. (2016)). Here, we show in-field, ground-based instrument checks conducted in Hangar N-159 at NASA Wallops Flight Facility, Wallops Island, USA, to ensure proper instrument operation and determine instrument precision. Power drawn from the aircraft remained under 50 *A* at all times and settled at approximately 40 *A*. The volumetric flow rate stabilized at 23 *SLPM* for a sample cell pressure regulated at 50.0 ± 0.2 *hPa* (measured 1-sigma @5Hz, excluding absolute error). Typical precision (standard deviation for 1s averaging) for ground-based operation is summarized in Tab. 2. These values are in good agreement with the values reported by Aerodyne, Inc..

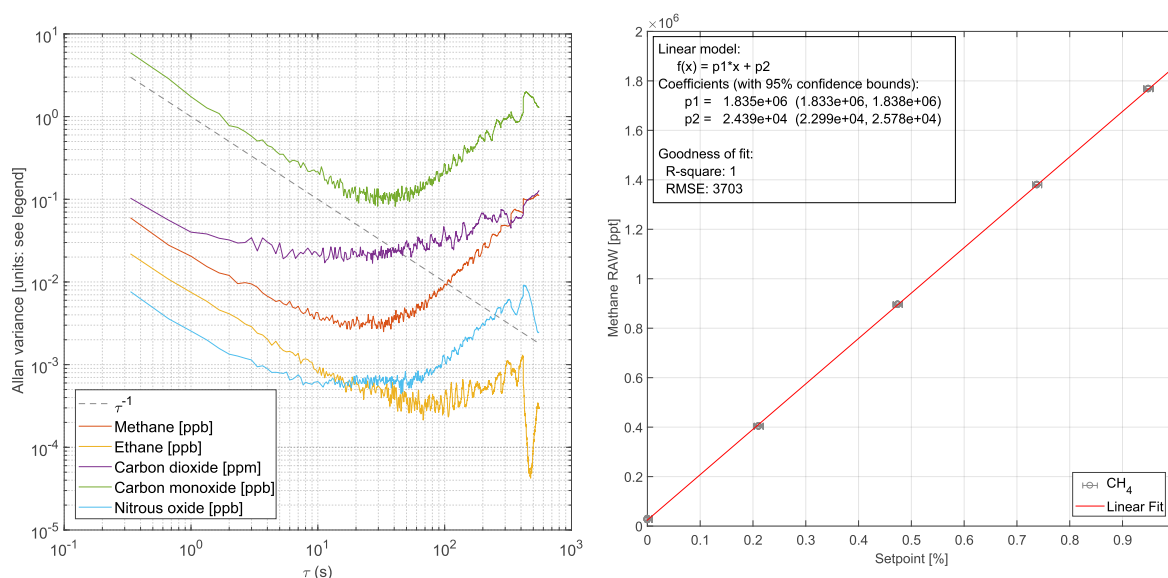


Figure 7. Allan variance for all measured chemical species during ground-based operation (left panel). The right panel demonstrates linearity for methane is within achievable error bounds during ground-based operation using the online calibration gas mixing system from Section 2.3.



Table 2. Achieved ground-based performance

Chemical species	H_2O	CH_4	C_2H_6	CO_2	CO	N_2O
Precision $1s - 1\sigma$	3.7 ppm	229 ppt	157 ppt	334 ppb	2.2 ppb	64 ppt

Fig. 7 shows the Allan variance for common averaging times τ for the individual trace gases monitored. For most species averaging up to 20s will decrease the signals standard deviation, before deteriorating effects (i.e. drift) occur. Figure 7 also addresses retrieved mixing ratio linearity. Linearity checks have been carried out for all species using the calibration system described in Section 2.3. All retrieved species are linear within error margin. CH_4 is used in Fig. 7 for demonstration purposes.

5 Typical shift parameters (as introduced in Sect. 3) for ground-based operation are depicted in Fig. 8 for the CH_4-H_2O and CO_2-CO-N_2O micro windows. These shift parameters can be considered as a tracer for instrument stability for both lasers. Overall spectral stability is in the range of $\pm 10^{-3} cm^{-1}$. Apart from expected low-frequency instability (due to thermal changes) on the lasers spectral output, high-frequency shifts are evident, including discontinuities. The source of these discontinuities remains unclear. They could be introduced by the software based frequency lock mechanism, by instabilities of the

10 laser itself or by timing changes in the sampling. The shape of the individual shifts match and so does their trend over time, which is a good indicator for a stable tuning rate during ground-based operation.

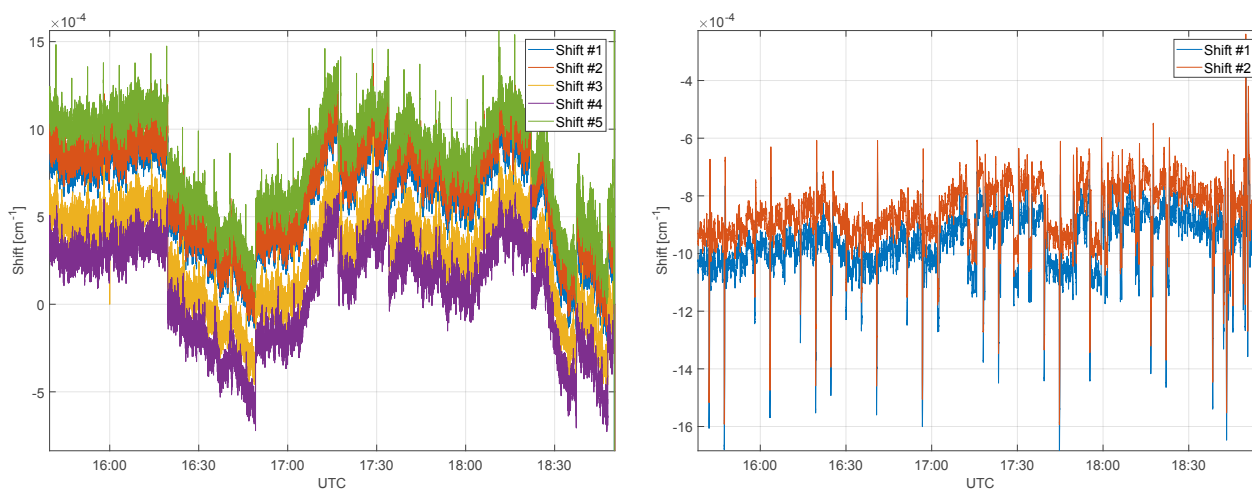


Figure 8. Spectral shifts for the CH_4-H_2O micro window (left) and the CO_2-CO-N_2O micro window (right). Spectral stability during ground-based operation is in the range of $\pm 10^{-3} cm^{-1}$.



5 Airborne instrument performance aboard NASA WFFs C-130

The instrument was successfully operated during 18 research flights aboard NASA Wallops Flight Facility's C-130 within the framework of the ACT-America fall 2017 field campaign. Other instrumentation in the ACT-America payload provided an excellent opportunity for instrument intercomparison. In situ CH_4 , CO_2 , and CO were measured using a PICARRO G2401-m cavity ring-down spectrometer, and in situ CO_2 , CH_4 , and $H_2O(g)$ were measured using a PICARRO G2301-m cavity ring-down analyzer. Precise C_2H_6 measurements were obtained by periodic flask samples by NOAA ESRL. Three onboard lidars, and in situ sensors measuring the meteorological state variables - winds, temperature, pressure and water vapor - completed the C130s instrument suite. Here we present data from a typical flight (10/03/2017) to demonstrate the airborne instrument performance through inter-comparison with well-established measurement techniques: the cavity ring-down PICARRO greenhouse gas analyzers and flask samples.

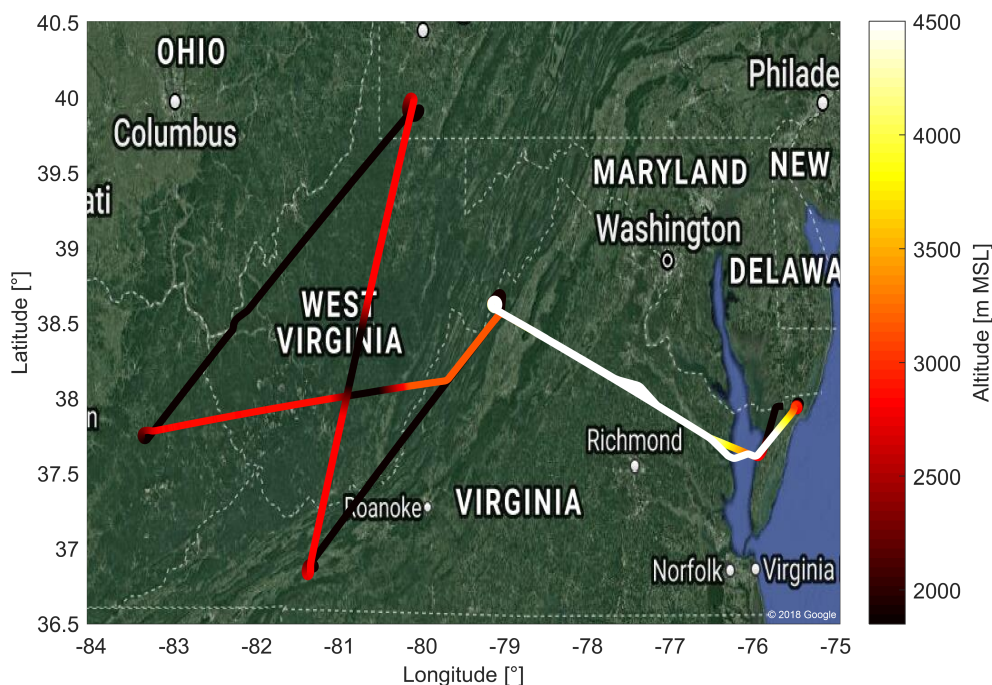


Figure 9. A typical fair-weather flight during ACT-America. This figure shows the flight pattern for Oct. 3, 2017 with color coded altitude. The flight includes two low-altitude (≈ 1000 ft AGL) legs downwind and upwind of parts of the Marcellus shale area. High-altitude transects between the two low-altitude legs include two en route descents and ascents in West Virginia.

10

As depicted in Fig. 9, the flight starts off from the eastern U.S. (Wallops Flight Facility, Virginia). A high-altitude transect to West-Virginia is followed by two low-altitude legs downwind and upwind of parts of the Marcellus shale area: a large shale gas extraction region. The transects between the two low-altitude legs are flown at high altitude to facilitate nadir lidar observation, with two en route descents and ascents near the center. Figure 10 depicts dry-air mixing ratios for CH_4 , C_2H_6 and



H_2O measured by the different instruments during the 5-hour flight. This figure provides evidence, that the QCLS, PICARRO and flask methane data are in good agreement over the entire flight. The center panel of Fig. 10 depicts the QCLS-retrieved C_2H_6 data superimposed with flask measurements. Here the QCLS-retrieved ethane data also matches the flask measurements (blue dots) within error margin. Unlike the QCLS, PICARRO and flask data are both sampled through an upstream dryer.

5 The lowermost panel of Fig. 10 provides water vapor mixing ratios obtained from an onboard hygrometer, from the G2301-m PICARRO analyzer and from the QCLS. The QCLS water vapor data is used to correct for water vapor effects during the retrieval of dry-air mixing ratios from the QCLS raw spectra as described in Sect. 3.1. By taking a closer look on the upper two panels, the benefit of simultaneously measuring several species can be readily identified. Figure 10 shows enhanced CH_4 without coinciding C_2H_6 enhancements for the first low-altitude leg. For the second low-altitude leg above the Marcellus area,

10 however, concurrent CH_4 and C_2H_6 enhancements suggest natural gas being the dominating source.

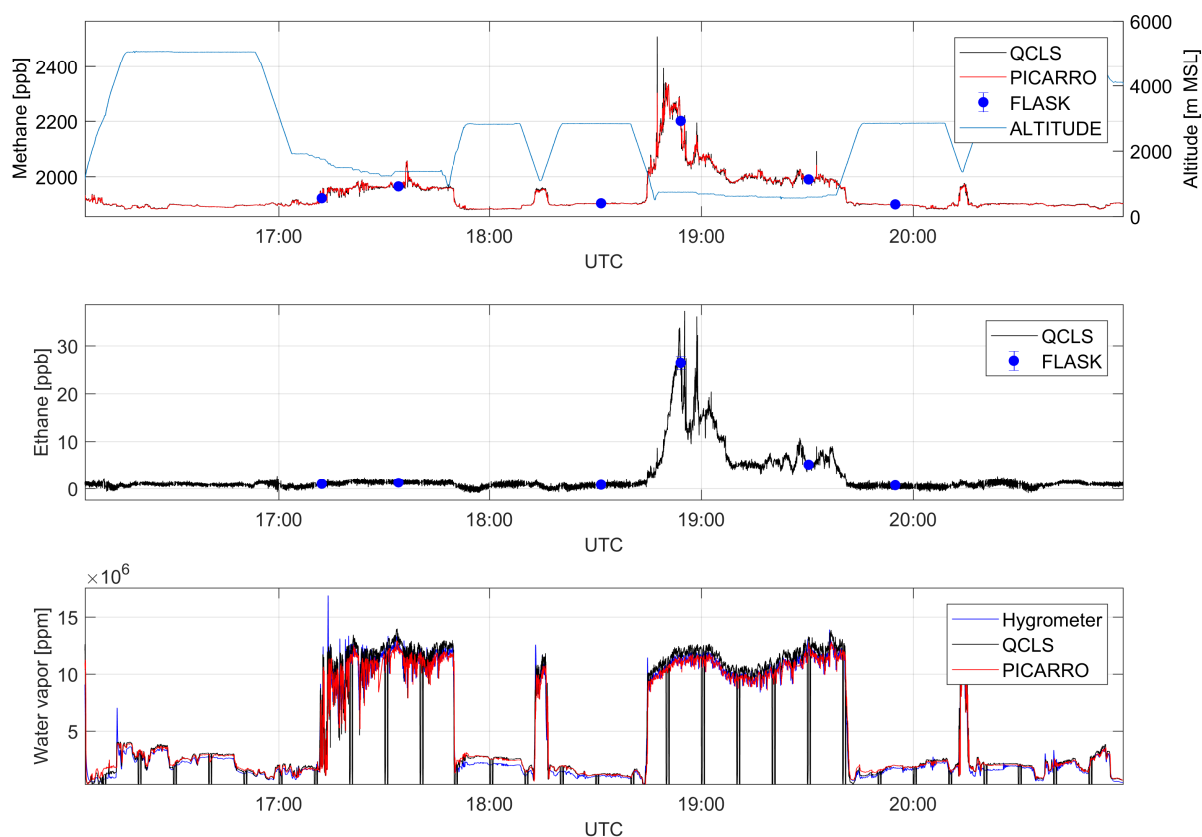


Figure 10. A direct comparison between dry-air mixing ratios retrieved from different measurement techniques for a complete flight on Oct. 3, 2017. Depicted are methane (uppermost panel), ethane (center panel) and water vapor (lowermost panel) mixing ratios. QCLS-retrieved methane data is in good accordance with PICARRO and flask data. QCLS-retrieved ethane data is in good agreement with flask data too. Water vapor sensed by an onboard hygrometer does differ from the PICARRO and QCLS data.



Time series for the species N_2O , CO and CO_2 are shown in Fig. 11. A good overall match between the different data sources can be identified. The N_2O time series matches available flask data to within ± 1 ppb. The CO_2 absorption is retrieved from a molecular transition of the $^{13}C^{16}O_2$ carbon dioxide isotopologue and scaled with its natural abundance of approximately 1.1% (Gordon et al., 2017)) to report total CO_2 . Despite the much lower abundance compared to $^{12}C^{16}O_2$ the QCLS-retrieved CO_2 data coincides with PICARRO data to within ± 2 ppm (1σ) after correcting for a constant bias (see below). QCLS-retrieved CO mixing ratios (center panel) agree with PICARRO-retrieved data to within ± 5 ppb (1σ). Fig. 11 suggests that in-flight precision depends on whether flying within the planetary boundary layer or above it. This is due to aircraft vibration excited by running engines and turbulence propagating into the instrument optics inducing slight changes in optical alignment. Typical in-flight precision figures for both regimes (standard deviation for 1s averaging) are summarized in Tab. 3. Total measurement uncertainty can be estimated from the uncertainty on the working standards, the uncertainty on calibration sequence evaluation, the uncertainty introduced by the H_2O correction, the precision of the instrument and errors due to drift. The relative error on the NOAA standards is stated with 0.2%, which expands to ~ 0.2 ppm and ~ 3.6 ppb for our CO_2 and CH_4

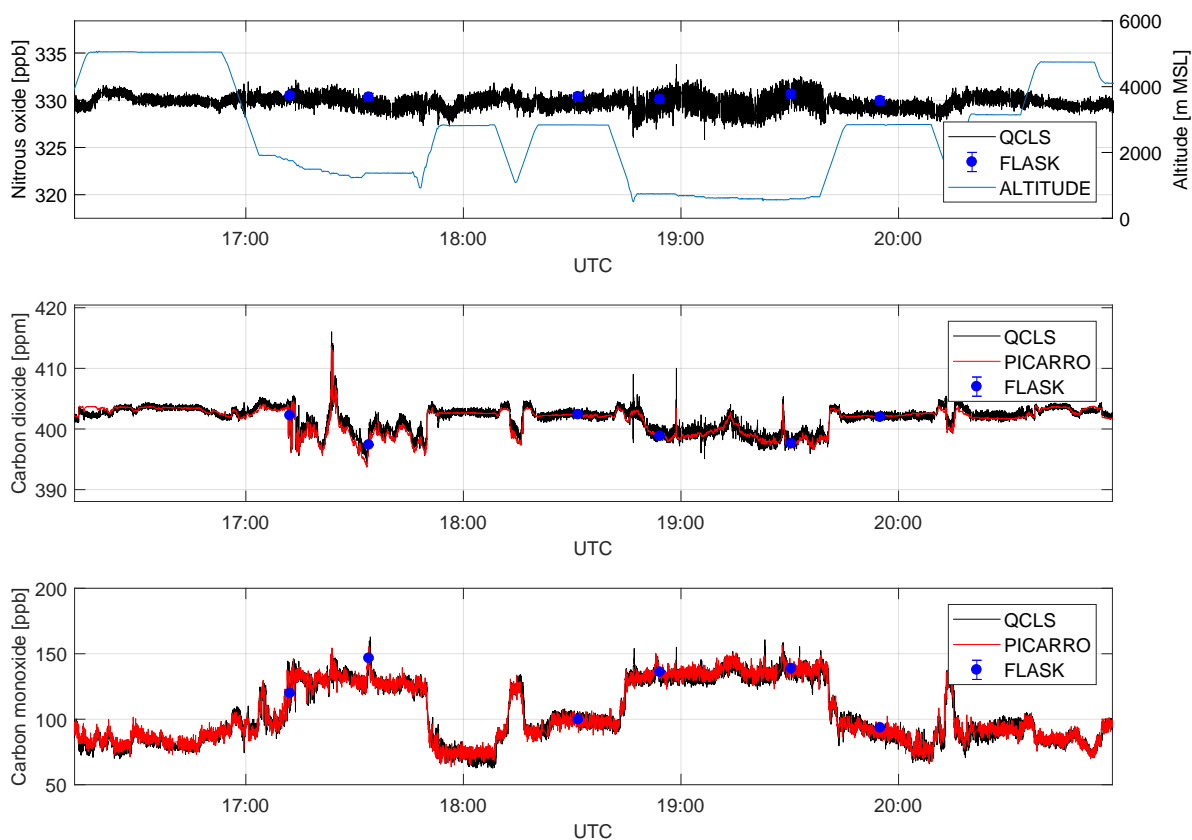


Figure 11. Dry-air mixing ratios retrieved from different measurement techniques for a complete flight on Oct. 3, 2017. Depicted are nitrous oxide (uppermost panel), carbon dioxide (center panel) and carbon monoxide (lowermost panel) mixing ratios.



Table 3. Typical in-flight performance including contributions to overall uncertainty. The total measurement uncertainty at 1s temporal resolution is given by the quadrature sum of the individual contributors.

Chemical species	H_2O	CH_4	C_2H_6	CO_2	CO	N_2O
Precision $1s - 1\sigma$ (within PBL)	16.2 ppm	740 ppt	205 ppt	460 ppb	2.2 ppb	439 ppt
Precision $1s - 1\sigma$ (above PBL)	2.5 ppm	300 ppt	146 ppt	182 ppb	1.4 ppb	208 ppt
Working standard reproducibility	—	0.03 ppb	—	0.1 ppm	—	—
Compared instrument uncertainty	—	—	1.5 ppb	—	5.0 ppb	0.4 ppb
Measurement calibration	—	2.0 ppb	0.5 ppb	0.9 ppm	5.0 ppb	0.5 ppb
H_2O correction	—	0.8 ppb	0.1 ppb	0.2 ppm	0.2 ppb	0.1 ppb
Total uncertainty	—	2.3 ppb	1.6 ppb	1.0 ppm	7.4 ppb	0.8 ppb

standard respectively. We found a bias constant for the whole measurement series of $\sim 2\text{ ppb}$ for CH_4 and $\sim 10\text{ ppm}$ for CO_2 between the QCLS and PICARRO/FLASK datasets. This constant bias has been corrected for. The large CO_2 bias most possibly results from a difference in the isotopic composition of the calibration standard relative to the sampled air. Since we are reporting retrieved mixing ratios relative to the WMO scale, however, only the working standard reproducibility contributes to the total uncertainty. Uncertainty on the other measured species is taken from the ACT-America dataset to allow for WMO traceability. The uncertainty on calibration sequence evaluation (see 2.3) is estimated with the double of the measurement precision and the uncertainty introduced by the H_2O correction is estimated from Eq. 1 using an assumed relative error on retrieved water vapor of 2%. Errors originating from instrument drift are considered negligible due to our frequent calibration strategy (see Section 2.3). The total uncertainty is given by the quadrature sum of the individual contributors, listed in Tab. 3.

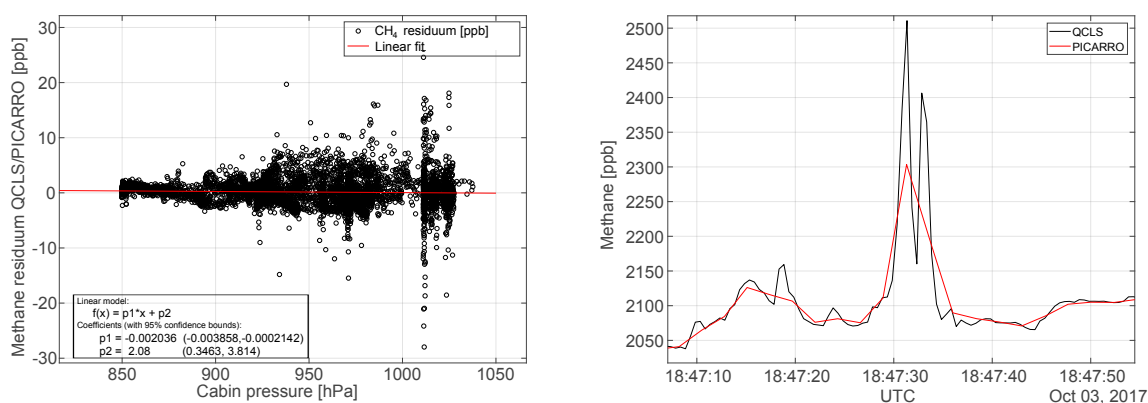


Figure 12. The left panel shows the cabin pressure dependence for a typical flight on Oct. 3, 2017. The large cabin pressure dependence in excess of 0.3 ppb hPa^{-1} reported by Pitt et al. (2016) could not be reproduced. The right hand side panel shows a temporal zoom on the methane data at 18:47 UTC to emphasize the benefit of high-frequency measurements.



A severe cabin pressure dependence in excess of 0.3 ppb hPa^{-1} in CH_4 mixing ratio has been previously reported for airborne Aerodyne TILDAS instrumentation (Pitt et al., 2016). We were not able to reproduce this large cabin pressure dependence during operation of the QCLS instrument aboard the C130 using the calibration strategy from Sect. 2.3. Figure 12 (left panel) shows the difference in CH_4 dry-air mixing ratio reported by the QCLS and the PICARRO instrument as a function of cabin pressure during the research flight described above. The large scatter results from different sampling patterns among the two instruments, hindering a one-to-one comparison of the QCLS measurements with the PICARRO. While the QCLS samples continuously with a frequency of 2 Hz (1.5 kHz sweep frequency), the PICARRO samples with a frequency of 0.5 Hz one species after the other. For CH_4 , for example, the PICARRO uses the first 0.5 s of the 2 s sampling time, implying that, for the

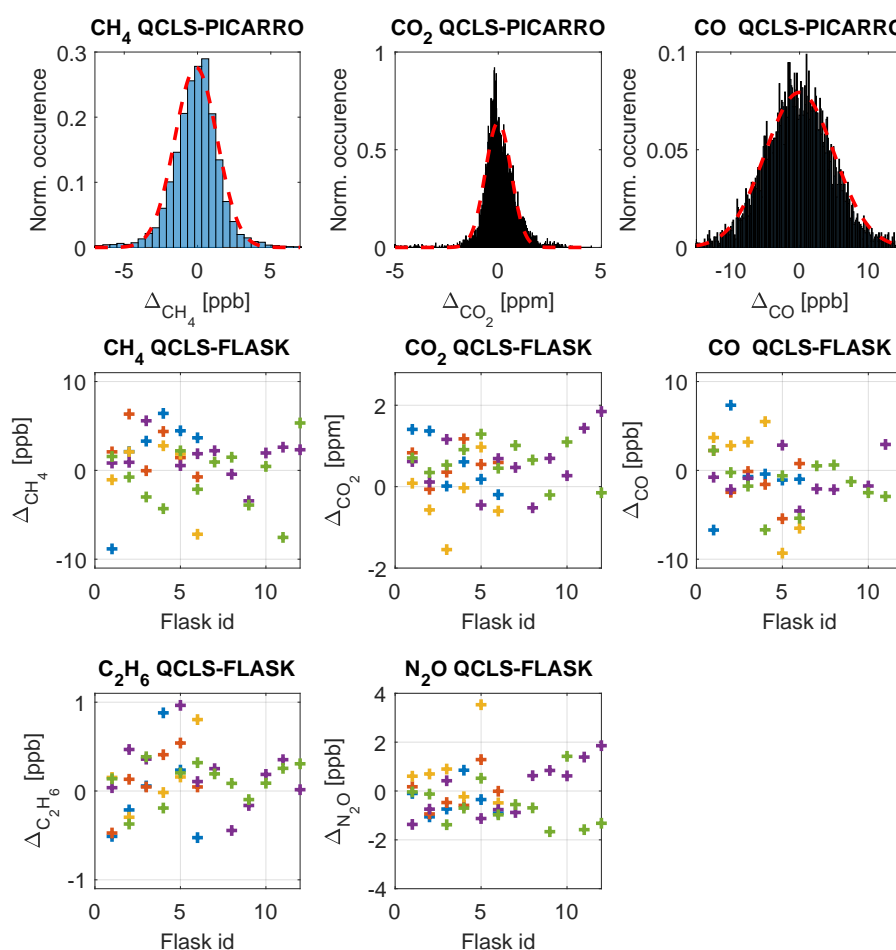


Figure 13. Comparison of QCLS derived mixing ratios to well-established in-flight PICARRO data and flask samples after correcting for a bias constant for the whole measurement series. Interpretation of the errors against flask samples is difficult for high-variability flight segments, due to the large flask sampling time. The residual plots show color-coded data from 5 typical flights on 10/03/2017, 10/11/2017, 10/14/2017, 10/18/2017 and 10/20/2017.



later 1.5 s, the PICARRO is insensitive to CH_4 . Therefore, it is difficult to mimic the PICARRO sampling by averaging the QCLS data as it would be required for a one-to-one comparison. Instead we decided to linearly interpolate QCLS data to the PICARRO timescale. The fast response time of the QCLS instrument allows for better sampling of spatially narrow plumes, as can be seen from the right hand side panel in Fig. 12. This panel zooms in on a relevant portion of the methane data from Fig. 10 and demonstrates that two mutually-separated plumes can be identified from the high frequency QCLS data at 18:47 UTC, where only a single enhancement can be seen from PICARRO data. Furthermore, absolute enhancement and area beneath the peak(s) differ for the two instruments, due to the different sampling patterns. Figure 13 compares the QCLS mixing ratios to the PICARRO instrument and to the flask samples after correcting for a bias constant for the whole measurement series. The upper panels show differences in retrieved mixing ratios between the QCLS and the cavity ring-down instrument for the flight on Oct. 3, 2017, exhibiting a near normal distribution. This hints towards residuals originating from random processes, i.e. noise. Although interpretation of the differences to flask samples is difficult for high-variability flight segments, the lower panels of Fig. 13 show a good agreement for five typical flights (10/03/2017, 10/11/2017, 10/14/2017, 10/18/2017, 10/20/2017) during the ACT-America campaign.

6 Conclusions

We adapted the commercially-available QCL/ICL based *Dual Laser Trace Gas Monitor* from *AERODYNE RESEARCH INC., Billerica, USA* for airborne operation and demonstrate successful operation over 18 research flights aboard NASA Wallops Flight Facility's C-130 during the ACT-America field campaign in fall 2017. Known cabin-pressure dependencies (Gvakharia et al. (2018); Pitt et al. (2016)) on the retrieved mixing ratios are effectively minimized using a frequent (5 to 10mins interval) two-point calibration approach obtained by flushing the sample cell with "zero" and "target" gases. This allows for a measurement duty cycle of $\geq 90\%$ when operating at sample flow rates near 23 SLPM . A custom retrieval software has been developed to allow for independent processing of raw spectra. We minimize retrieval artifacts by introducing a new way to handle spectral shifts. We reduce fitting residuals by implementing open path water vapor absorption using an auxiliary sensor mounted inside the instruments optics compartment. Apart from low frequency laser instability we identify high frequency "jumps" on the spectral axis, possibly due to the instruments frequency lock mechanism. In-flight performance has been assessed using data obtained during the research flight on the 3rd Oct. 2017 above the eastern U.S.. We identify two precision regimes whether flying within the planetary boundary layer or above, due to aircraft vibration propagating into the instrument optics and related slight changes in optical alignment. Typical in-flight precision figures for boundary layer flights (standard deviation for 1s averaging) are 740 ppt , 205 ppt , 460 ppb , 2.2 ppb , 137 ppt , 16 ppm for CH_4 , C_2H_6 , CO_2 , CO , N_2O and H_2O respectively. Precision figures improve to approximately the half for flights above the PBL. We estimate a total measurement uncertainty of 2.3 ppb , 1.6 ppb , 1.0 ppm , 7.4 ppb and 0.8 ppb in CH_4 , C_2H_6 , CO_2 , CO and N_2O , respectively. We demonstrate an excellent agreement to concurrent flask sample and cavity-ringdown measurements within combined measurement uncertainty for all targeted species. The instrument retrieves carbon dioxide mixing ratios via a $^{13}C^{16}O_2$ absorption line and is thus



shown to be capable of detecting isotopologue level mixing ratios, which will be picked up in the near future to modify the instrument for airborne isotope ratio analysis.

Code and data availability. Software code and data are available from the authors upon request.

Competing interests. The authors are not aware of any competing interests.

- 5 *Acknowledgements.* We thank DLR VO-R for funding the young investigator research group "Greenhouse Gases". We also acknowledge funding from BMBF under project "AIRSPACE" (Grant-no. FKZ01LK170). The Atmospheric Carbon and Transport (ACT) - America project is a NASA Earth Venture Suborbital 2 project funded by NASA's Earth Science Division (Grant NNX15AG76G to Penn State). Aircraft operations and U.S. investigators were funded via the ACT-America project. We greatly appreciate continuous support from Hans Schlager and Markus Rapp from DLR. We further thank the GLORIA team, especially Christof Piesch and Hans Nordmeyer at the Karlsruhe
- 10 Institute of Technology (KIT) for enabling us pressure testing the rack-mounted QCLS in a climate chamber. We also thank Paul Stock and Monika Scheibe from DLR and Martin Nowicki from NASA WFF for engineering support. Furthermore we would like to thank everyone involved during the ACT-America field campaigns for their relentless dedication and the helpful discussions, especially Alan Fried, Bing Lin, John Nowak, Linda D. Thompson, Charles E. Juenger. A special thanks to Mark Zahniser and Dave Nelson from Aerodyne Inc. for their valuable support whenever help was needed.



References

- Abrarov, S. and Quine, B.: A Rational Approximation for Efficient Computation of the Voigt Function in Quantitative Spectroscopy, 7, 2015.
- Barkley, Z. R., Lauvaux, T., Davis, K. J., Deng, A., Miles, N. L., Richardson, S. J., Cao, Y., Sweeney, C., Karion, A., Smith, M., Kort, E. A., Schwietzke, S., Murphy, T., Cervone, G., Martins, D., and Maasackers, J. D.: Quantifying methane emissions from natural gas production in north-eastern Pennsylvania, *Atmospheric Chemistry and Physics*, 17, 13 941–13 966, <https://doi.org/10.5194/acp-17-13941-2017>, <https://www.atmos-chem-phys.net/17/13941/2017/>, 2017.
- Beck, M., Hofstetter, D., Aellen, T., Faist, J., Oesterle, U., Ilegems, M., Gini, E., and Melchior, H.: Continuous Wave Operation of a Mid-Infrared Semiconductor Laser at Room Temperature, *Science*, 295, 301–305, <https://doi.org/10.1126/science.1066408>, <http://science.sciencemag.org/content/295/5553/301>, 2002.
- 10 Cambaliza MOL, Shepson PB, B. J. C. D. S. B. S. C. e. a.: Quantification and source apportionment of the methane emission flux from the city of Indianapolis, *Elem Sci Anth.*, 3, <https://doi.org/10.12952/journal.elementa.000037>, <https://www.atmos-meas-tech.net/9/4737/2016/>, 2015.
- Capasso, F.: High-performance midinfrared quantum cascade lasers, 49, 1102–, 2010.
- Catoire, V., Robert, C., Chartier, M., Jacquet, P., Guimbaud, C., and Krysztofciak, G.: The SPIRIT airborne instrument: a three-channel infrared absorption spectrometer with quantum cascade lasers for in situ atmospheric trace-gas measurements, *Applied Physics B*, 123, 244, <https://doi.org/10.1007/s00340-017-6820-x>, <https://doi.org/10.1007/s00340-017-6820-x>, 2017.
- 15 Chen, H., Winderlich, J., Gerbig, C., Hofer, A., Rella, C. W., Crosson, E. R., Van Pelt, A. D., Steinbach, J., Kolle, O., Beck, V., Daube, B. C., Gottlieb, E. W., Chow, V. Y., Santoni, G. W., and Wofsy, S. C.: High-accuracy continuous airborne measurements of greenhouse gases (CO₂ and CH₄) using the cavity ring-down spectroscopy (CRDS) technique, *Atmospheric Measurement Techniques*, 3, 375–386, <https://doi.org/10.5194/amt-3-375-2010>, <https://www.atmos-meas-tech.net/3/375/2010/>, 2010.
- 20 Filges, A., Gerbig, C., Chen, H., Franke, H., Klaus, C., and Jordan, A.: The IAGOS-core greenhouse gas package: a measurement system for continuous airborne observations of CO₂, CH₄, H₂O and CO, *Tellus B: Chemical and Physical Meteorology*, 67, 27 989, <https://doi.org/10.3402/tellusb.v67.27989>, <https://doi.org/10.3402/tellusb.v67.27989>, 2015.
- Gordon, I., Rothman, L., Hill, C., Kochanov, R., Tan, Y., Bernath, P., Birk, M., Boudon, V., Campargue, A., Chance, K., Drouin, B., Flaud, J.-M., Gamache, R., Hodges, J., Jacquemart, D., Perevalov, V., Perrin, A., Shine, K., Smith, M.-A., Tennyson, J., Toon, G., Tran, H., Tyuterev, V., Barbe, A., Császár, A., Devi, V., Furtenbacher, T., Harrison, J., Hartmann, J.-M., Jolly, A., Johnson, T., Karman, T., Kleiner, I., Kyuberis, A., Loos, J., Lyulin, O., Massie, S., Mikhailenko, S., Moazzen-Ahmadi, N., Müller, H., Naumenko, O., Nikitin, A., Polyansky, O., Rey, M., Rotger, M., Sharpe, S., Sung, K., Starikova, E., Tashkun, S., Auwera, J. V., Wagner, G., Wilzewski, J., Wcisło, P., Yu, S., and Zak, E.: The HITRAN2016 molecular spectroscopic database, *Journal of Quantitative Spectroscopy and Radiative Transfer*, 203, 3 – 69, <https://doi.org/https://doi.org/10.1016/j.jqsrt.2017.06.038>, <http://www.sciencedirect.com/science/article/pii/S0022407317301073>, HITRAN2016 Special Issue, 2017.
- 30 Gvakharia, A., Kort, E. A., Smith, M. L., and Conley, S.: Testing and evaluation of a new airborne system for continuous N₂O, CO₂, CO, and H₂O measurements: the Frequent Calibration High-performance Airborne Observation System (FCHAOS), *Atmospheric Measurement Techniques Discussions*, 2018, 1–22, <https://doi.org/10.5194/amt-2018-201>, <https://www.atmos-meas-tech-discuss.net/amt-2018-201/>, 2018.
- 35



- Harazono, Y., Iwata, H., Sakabe, A., Ueyama, M., Takahashi, K., Nagano, H., Nakai, T., and Kosugi, Y.: Effects of water vapor dilution on trace gas flux, and practical correction methods, *Journal of Agricultural Meteorology*, 71, 65–76, <https://doi.org/10.2480/agrmet.D-14-00003>, 2015.
- Harrison, J. J., Allen, N. D., and Bernath, P. F.: Infrared absorption cross sections for ethane (C₂H₆) in the 3 μ m region, *Journal of Quantitative Spectroscopy and Radiative Transfer*, 111, 357 – 363, <https://doi.org/https://doi.org/10.1016/j.jqsrt.2009.09.010>, <http://www.sciencedirect.com/science/article/pii/S0022407309002866>, 2010.
- IPCC, .: Climate Change 2014: Synthesis Report. Contribution of Working Groups I, II and III to the Fifth Assessment Report of the Intergovernmental Panel on Climate Change [Core Writing Team, R.K. Pachauri and L.A. Meyer (eds.)], IPCC, Geneva, Switzerland, 2014.
- 10 Kim, M., Bewley, W. W., Canedy, C. L., Kim, C. S., Merritt, C. D., Abell, J., Vurgaftman, I., and Meyer, J. R.: High-power continuous-wave interband cascade lasers with 10 active stages, *Opt. Express*, 23, 9664–9672, <https://doi.org/10.1364/OE.23.009664>, <http://www.opticsexpress.org/abstract.cfm?URI=oe-23-8-9664>, 2015.
- Klemm, O., Hahn, M. K., and Giehl, H.: Airborne, Continuous Measurement of Carbon Monoxide in the Lower Troposphere, *Environmental Science & Technology*, 30, 115–120, <https://doi.org/10.1021/es950145j>, <https://doi.org/10.1021/es950145j>, 1996.
- 15 Kooijmans, L. M. J., Uitslag, N. A. M., Zahniser, M. S., Nelson, D. D., Montzka, S. A., and Chen, H.: Continuous and high-precision atmospheric concentration measurements of COS, CO₂, CO and H₂O using a quantum cascade laser spectrometer (QCLS), *Atmospheric Measurement Techniques*, 9, 5293–5314, <https://doi.org/10.5194/amt-9-5293-2016>, <https://www.atmos-meas-tech.net/9/5293/2016/>, 2016.
- Marquardt, D.: An Algorithm for Least-Squares Estimation of Nonlinear Parameters, *Journal of the Society for Industrial and Applied Mathematics*, 11, 431–441, <https://doi.org/10.1137/0111030>, <https://doi.org/10.1137/0111030>, 1963.
- 20 McManus, J. B., Zahniser, M. S., and Nelson, D. D.: Dual quantum cascade laser trace gas instrument with astigmatic Herriott cell at high pass number, *Appl. Opt.*, 50, A74–A85, <https://doi.org/10.1364/AO.50.000A74>, <http://ao.osa.org/abstract.cfm?URI=ao-50-4-A74>, 2011.
- McManus, J. B., Nelson, D. D., and Zahniser, M. S.: Design and performance of a dual-laser instrument for multiple isotopologues of carbon dioxide and water, *Opt. Express*, 23, 6569–6586, <https://doi.org/10.1364/OE.23.006569>, <http://www.opticsexpress.org/abstract.cfm?URI=oe-23-5-6569>, 2015.
- 25 O’Shea, S. J., Allen, G., Fleming, Z. L., Bauguitte, S. J., Percival, C. J., Gallagher, M. W., Lee, J., Helfter, C., and Nemitz, E.: Area fluxes of carbon dioxide, methane, and carbon monoxide derived from airborne measurements around Greater London: A case study during summer 2012, *Journal of Geophysical Research: Atmospheres*, 119, 4940–4952, <https://doi.org/10.1002/2013JD021269>, <https://agupubs.onlinelibrary.wiley.com/doi/abs/10.1002/2013JD021269>, 2013.
- Peischl, J., Karion, A., Sweeney, C., Kort, E. A., Smith, M. L., Brandt, A. R., Yeskoo, T., Aikin, K. C., Conley, S. A., Gvakharia, A., Trainer, M., Wolter, S., and Ryerson, T. B.: Quantifying atmospheric methane emissions from oil and natural gas production in the Bakken shale region of North Dakota, *Journal of Geophysical Research: Atmospheres*, 121, 6101–6111, <https://doi.org/10.1002/2015JD024631>, <https://agupubs.onlinelibrary.wiley.com/doi/abs/10.1002/2015JD024631>, 2015.
- 30 Pitt, J. R., Le Breton, M., Allen, G., Percival, C. J., Gallagher, M. W., Bauguitte, S. J.-B., O’Shea, S. J., Muller, J. B. A., Zahniser, M. S., Pyle, J., and Palmer, P. I.: The development and evaluation of airborne in situ N₂O and CH₄ sampling using a quantum cascade laser absorption spectrometer (QCLAS), *Atmospheric Measurement Techniques*, 9, 63–77, <https://doi.org/10.5194/amt-9-63-2016>, <https://www.atmos-meas-tech.net/9/63/2016/>, 2016.



- Ravishankara, A. R., Daniel, J. S., and Portmann, R. W.: Nitrous Oxide (N₂O): The Dominant Ozone-Depleting Substance Emitted in the 21st Century, *Science*, 326, 123–125, <https://doi.org/10.1126/science.1176985>, <http://science.sciencemag.org/content/326/5949/123>, 2009.
- Richter, D., Weibring, P., Walega, J. G., Fried, A., Spuler, S. M., and Taubman, M. S.: Compact highly sensitive multi-species airborne mid-IR spectrometer, *Applied Physics B*, 119, 119–131, <https://doi.org/10.1007/s00340-015-6038-8>, <https://doi.org/10.1007/s00340-015-6038-8>, 5 2015.
- Rothman, L. S., Gordon, I. E., Babikov, Y., Barbe, A., Chris Benner, D., Bernath, P. F., Birk, M., Bizzocchi, L., Boudon, V., Brown, L. R., Campargue, A., Chance, K., Cohen, E. A., Coudert, L. H., Devi, V. M., Drouin, B. J., Fayt, A., Flaud, J.-M., Gamache, R. R., Harrison, J. J., Hartmann, J.-M., Hill, C., Hodges, J. T., Jacquemart, D., Jolly, A., Lamouroux, J., Le Roy, R. J., Li, G., Long, D. A., Lyulin, O. M., Mackie, C. J., Massie, S. T., Mikhailenko, S., Müller, H. S. P., Naumenko, O. V., Nikitin, A. V., Orphal, J., Perevalov, V., Perrin, A., 10 Polovtseva, E. R., Richard, C., Smith, M. A. H., Starikova, E., Sung, K., Tashkun, S., Tennyson, J., Toon, G. C., Tyuterev, V. G., and Wagner, G.: The HITRAN2012 molecular spectroscopic database, *JQSRT*, 130, 4–50, <https://doi.org/10.1016/j.jqsrt.2013.07.002>, 2013.
- Santoni, G. W., Daube, B. C., Kort, E. A., Jiménez, R., Park, S., Pittman, J. V., Gottlieb, E., Xiang, B., Zahniser, M. S., Nelson, D. D., McManus, J. B., Peischl, J., Ryerson, T. B., Holloway, J. S., Andrews, A. E., Sweeney, C., Hall, B., Hints, E. J., Moore, F. L., Elkins, J. W., Hurst, D. F., Stephens, B. B., Bent, J., and Wofsy, S. C.: Evaluation of the airborne quantum cascade laser spectrometer (QCLS) measurements of the carbon and greenhouse gas suite *CO*₂, *CH*₄, *N*₂*O*, and CO during the CalNex and HIPPO campaigns, *Atmospheric Measurement Techniques*, 7, 1509–1526, <https://doi.org/10.5194/amt-7-1509-2014>, <https://www.atmos-meas-tech.net/7/1509/2014/>, 2014.
- Simpson, I. J., Sulbaek Andersen, M. P., Meinardi, S., Bruhwiler, L., Blake, N. J., Helmig, D., Rowland, F. S., and Blake, D. R.: Long-term decline of global atmospheric ethane concentrations and implications for methane, *Nature*, 488, 490 EP –, <http://dx.doi.org/10.1038/nature11342>, 2012.
- 20 Smith, M. L., Kort, E. A., Karion, A., Sweeney, C., Herndon, S. C., and Yacovitch, T. I.: Airborne Ethane Observations in the Barnett Shale: Quantification of Ethane Flux and Attribution of Methane Emissions, *Environmental Science & Technology*, 49, 8158–8166, <https://doi.org/10.1021/acs.est.5b00219>, <https://doi.org/10.1021/acs.est.5b00219>, PMID: 26148554, 2015.
- Vurgaftman, I., Weih, R., Kamp, M., Meyer, J. R., Canedy, C. L., Kim, C. S., Kim, M., Bewley, W. W., Merritt, C. D., Abell, J., and Höfling, S.: Interband cascade lasers, *Journal of Physics D: Applied Physics*, 48, 123 001, <http://stacks.iop.org/0022-3727/48/i=12/a=123001>, 2015.
- 25 Zellweger, C., Emmenegger, L., Firdaus, M., Hatakka, J., Heimann, M., Kozlova, E., Spain, T. G., Steinbacher, M., van der Schoot, M. V., and Buchmann, B.: Assessment of recent advances in measurement techniques for atmospheric carbon dioxide and methane observations, *Atmospheric Measurement Techniques*, 9, 4737–4757, <https://doi.org/10.5194/amt-9-4737-2016>, <https://www.atmos-meas-tech.net/9/4737/2016/>, 2016.